ACS Catalysis

Research Article

pubs.acs.org/acscatalysis

CO Oxidation on the Pd(111) Surface

Zhiyao Duan and Graeme Henkelman*

Department of Chemistry and the Institute for Computational Engineering and Sciences, The University of Texas at Austin, Austin, Texas 78712-0165, United States

ABSTRACT: Under technologically relevant oxygen-rich conditions, the reaction mechanism of CO oxidation over transition metals can be complicated by the formation of oxides. Questions of whether the active surface for CO oxidation is a pristine metal, a surface oxide, or a bulk oxide is still under active debate. In this study, density functional theory calculations are used to model CO oxidation on the Pd(111) surface. Our results show that a thin layer of Pd_5O_4 surface oxide is stable under catalytically relevant gas-phase conditions. Three-fold oxygen atoms in the surface are found to react with gas-phase CO molecules following an Eley−Rideal reaction mechanism. Such CO oxidation reduces the surface oxide, but the oxide can be replenished by O_2 dissociation. Kinetic analysis shows that experimentally observed reaction conditions, that are uninhibited by CO and limited only by mass transfer, correspond to a surface oxide phase with CO oxidation occurring though the Eley−Rideal mechanism. Under steady-state operating conditions, the continuous formation and decomposition of the surface oxide is expected and is key to the high CO oxidation rate on Pd(111).

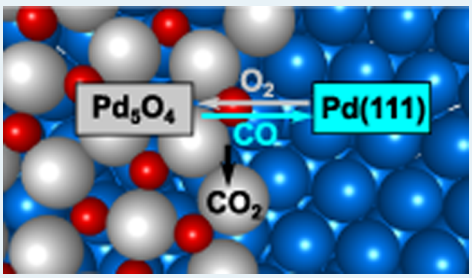

KEYWORDS: *CO oxidation, palladium, catalysis, density functional theory, Pd_5O_4 surface oxide, constrained equilibrium method, surface phase diagram, reaction kinetics*

1. INTRODUCTION

Pd is a widely used catalyst in catalytic converters for the oxidation of CO and unburnt fuel in automotive exhaust gases. A fundamental understanding of CO oxidation on a Pd catalyst has been gained through model studies using single crystal surfaces under ultrahigh vacuum (UHV) conditions.[1−4] It is generally believed that CO oxidation proceeds via a Langmuir−Hinshelwood (LH) mechanism under UHV conditions, whereby both reactants (CO and O_2) first adsorb on the metal surface and then subsequently react to form CO_2. Practically, Pd catalysts operate at ambient pressure under oxygen-rich conditions as a result of modern high air:fuel ratio engines. The high oxygen pressure may cause oxygen-rich phases to form, including oxygen-rich chemisorption structures, surface oxide thin films, and bulk oxide. It is expected that a change in the catalyst surface, and especially a phase transition from metal to oxide, will dramatically influence the catalytic reaction mechanism. Due to the complex nature of the catalyst surface under realistic conditions and the difficulties of characterization tools in achieving atomic-scale resolution under ambient pressure and elevated temperature, it is unclear whether the reactive surface is the pristine metal surface, a surface oxide thin film, or a bulk oxide (PdO) overlayer.[5]

CO oxidation over Pd(100) is one of the most well-studied model catalysts under ambient pressure conditions, both experimentally and theoretically. Using a combined flow reactor and high-pressure scanning tunneling microscopy (STM), Hendriksen et al. found that an increase in reactivity of CO oxidation coincided with oxide formation on Pd(100) surface.[6] The reaction mechanism of CO oxidation on the oxide was proposed to follow the Mars-Van Krevelen (MvK) mechanism, in which the oxide is continually consumed and reformed. Recent studies using high-pressure surface X-ray diffraction (SXRD)[7,8] and ambient-pressure X-ray photoelectron spectroscopy (AP-XPS)[9,10] also found the catalytic activity significantly increased when the surface was oxidized to the $(\sqrt{5}\times\sqrt{5})R27°$ surface oxide[11,12] and/or to the PdO bulk oxide. Theoretically, using constrained thermodynamics and first-principles kinetic Monte Carlo (KMC) based on energetics calculated by density functional theory (DFT), the presence and the catalytic activity of the $(\sqrt{5}\times\sqrt{5})R27°$ surface oxide were confirmed under technically relevant conditions.[13−15]

Fewer studies have been performed on the Pd(111) surface, and less is known about its reactivity. In a recent AP-XPS study,[16] Toyoshima et al. found that the two-dimensional Pd_5O_4 surface oxide[17−19] starts to form at elevated temperatures (300 °C—400 °C) and that the reactivity is enhanced in the presence of the surface oxide. It was suggested that the active oxygen species is the 3-fold coordinated oxygen atom in the Pd_5O_4 surface oxide layer or a chemisorbed oxygen atom on Pd(111); distinguishing between these species was not possible because of their similar 1*s* electron binding energies. In the same study, the catalytic activity was found to be suppressed when the surface was further oxidized to form oxide clusters or a PdO bulk oxide layer. Other studies, however, disagree with the interpreted high activity of the oxide phase. Altman and coworkers found the $(\sqrt{5}\times\sqrt{5})R27°$ surface oxide and the PdO bulk oxide were less reactive than a (2×2) chemisorbed

Received: May 4, 2014
Revised: August 11, 2014

   dx.doi.org/10.1021/cs5006025 | *ACS Catal.* 2014, 4, 3435−3443

phase.[20] Goodman and co-workers, in a combined polarization modulation-infrared reflection absorption spectroscopy (PM-IRAS) and kinetics study, assigned the most reactive phase to a chemisorbed atomic oxygen, with a low coverage of CO, that transiently formed during the phase transition from a CO-poisoned metallic surface to a Pd oxide phase.[21−25]

In this work, DFT calculations provide a microscopic model of CO oxidation on the Pd(111) surface. Specifically, we use a constrained equilibrium approach[13,26] to construct a surface phase diagram and calculate the most stable surface structures under reaction conditions. It is found that, under technologically relevant conditions, the phase boundary between the Pd_5O_4 surface oxide and CO-covered metallic surface is the most relevant surface structure responsible the high catalytic activity. A kinetic study was then performed to investigate CO oxidation on the surface oxide. Combining the kinetic study with our thermodynamic stability considerations, a particular region in the surface phase diagram in which the surface oxide is able to form and decompose was found to have a high activity toward CO oxidation.

2. COMPUTATIONAL METHODS

2.1. Surface Phase Diagram. Surface phase diagrams, constructed from DFT calculations, are useful for the identification of relevant surface structures at technological gas pressures as well as phase coexistence regions where high catalytic activity is expected.[13] To calculate a surface phase diagram, the relative stability of CO and O adsorption structures on the Pd(111) surface first needs to be determined. The Gibbs free energy of adsorption (ΔG^{ads}) is evaluated as a function of the chemical potential of CO (μ_{CO}) and O (μ_O)

$$\Delta G^{ads} = -\frac{1}{A}[G^{surf}_{O,CO/Pd(111)} - G^{surf}_{Pd(111)} - \Delta N_{Pd}\mu^{bulk}_{Pd} - N_O\mu_O - N_{CO}\mu_{CO})] \quad (1)$$

Here A is the surface area, $G^{surf}_{O,CO/Pd(111)}$ is the Gibbs free energy of the Pd(111) surface with N_O adsorbed O atoms and N_{CO} adsorbed CO molecules, $G^{surf}_{Pd(111)}$ is the Gibbs free energy of clean Pd(111) surface, and ΔN_{Pd} is the difference in number of Pd atoms in the adsorption surface (including possible surface reconstruction) and the clean surface; the reference energy for Pd atoms μ_{Pd} is from the bulk reservoir. The chemical potentials of O and CO are determined from thermodynamic equilibrium with gas-phase reservoirs. Thus, the O and CO chemical potentials depend on temperature and pressure according to

$$\mu_O(T, p_{O_2}) = \frac{1}{2}\left[E^{tot}_{O_2} + \tilde{\mu}_{O_2}(T, p^0) + k_B T \ln\frac{p_{O_2}}{p^0}\right] \quad (2)$$

and

$$\mu_{CO}(T, p_{CO}) = E^{tot}_{CO} + \tilde{\mu}_{CO}(T, p^0) + k_B T \ln\frac{p_{CO}}{p^0} \quad (3)$$

where p^0 is the standard pressure, and $\tilde{\mu}_{O_2}(T, p^0)$ and $\tilde{\mu}_{CO}(T, p^0)$ are the chemical potentials at p^0, which are obtained from thermodynamical tables.[27] The temperature- and pressure-dependent terms in eqs 2 and 3 are further combined into one term, so that the chemical potentials are $\mu_O = 1/2E^{tot}_{O_2} + \Delta\mu_O(T, p)$ and $\mu_{CO} = E^{tot}_{CO} + \Delta\mu_{CO}(T, p)$. Substituting the above chemical potential expressions of gas-phase molecules into eq 1 and approximating the difference of the Gibbs free energy of the clean, adsorbate covered surfaces and of the bulk system in eq 1 by the DFT total energies gives ΔG^{ads} is

$$\Delta G^{ads} \approx -\frac{1}{A}\tilde{E}^{bind}_{O,CO/Pd(111)} + \frac{N_O}{A}\Delta\mu_O + \frac{N_{CO}}{A}\Delta\mu_{CO} \quad (4)$$

where $\tilde{E}^{bind}_{O,CO/Pd(111)}$ (the binding energy of O and CO) is defined as

$$\tilde{E}^{bind}_{O,CO/Pd(111)} = E^{tot}_{O,CO/Pd(111)} - E^{tot}_{Pd(111)} - \Delta N_{Pd}E^{tot}_{Pd} - \frac{N_O}{2}E^{tot}_{O_2} - N_{CO}E^{tot}_{CO} \quad (5)$$

The adsorption structures are stable if $\Delta G^{ads} > 0$. Hence, the most stable adsorption structure at a given condition ($\Delta\mu_O$, $\Delta\mu_{CO}$) has the largest $\Delta G^{ads} > 0$. The surface diagram can then be constructed to show the most stable structure as a function of catalytic conditions. Since ΔG^{ads} depends on two independent variables, the surface phase diagram is two-dimensional, with regions representing stable phases and dividing lines between them representing phase boundaries. As well as various adsorption structures, the Pd_5O_4 surface oxide, and the formation of a bulk PdO oxide layer were also considered when constructing the diagram. The neglected contributions to the Gibbs free energy of adsorption are the pV term, the configurational entropy S^{conf} in the adsorbate overlayer, and the vibrational free energy change of molecules upon adsorption $\Delta F^{ads,vib}$. The uncertainty introduced by these approximations has been assessed in previous publications[13,26] and found to only marginally modify the boundaries of stable phases. Recent work by Campbell,[28] however, shows that at high coverage, adsorbed molecules can retain about 2/3 of their gas phase entropy. Simply neglecting the entropy of the adsorbed molecules as done in this study and previously in refs 26 and 13 could lead to a significant underestimation of the calculated stability of the CO chemisorption phases. The entropy of adsorbed molecules will be further discussed in our calculations of surface phase diagrams.

Combining the condition of PdO formation in an O_2 gas environment and of PdO decomposition in a CO environment, the stability criterion for PdO is

$$\Delta\mu_{CO} - \Delta\mu_O < -2\Delta E^f_{PdO} + \Delta E^f_{CO_2} \quad (6)$$

Here, $\Delta E^f_{PdO} \approx E^{tot}_{PdO} - E^{tot}_{Pd} - 1/2E^{tot}_{O_2}$ is the formation energy of PdO at 0 K, and $\Delta E^f_{CO_2} = E^{tot}_{CO_2} - E^{tot}_{CO} - 1/2E^{tot}_{O_2}$ is the formation energy of CO_2 from CO and O_2. The calculated values of ΔE^f_{PdO} and $\Delta E^f_{CO_2}$ along with corresponding experimental values are listed in Table 1. In calculating $\Delta E^f_{CO_2}$, the chemical potential of CO_2 is approximated by the DFT total energy E_{CO_2}. The error introduced by the approximation is primarily due to the vibrational free energy of CO_2, which has been previously estimated to be on the order of 0.3 eV.[13] While the magnitude of this variation in $\Delta E^f_{CO_2}$ is

Table 1. Calculated Formation Energies of PdO and CO_2 (eV)

	RPBE	PW91	experiment[13]
ΔE^f_{PdO}	−0.73	−0.88	−0.97
$\Delta E^f_{CO_2}$	−3.05	−3.34	−3.00

dx.doi.org/10.1021/cs5006025 | ACS Catal. 2014, 4, 3435−3443

not negligible and tends to make PdO less stable, it does not affect the conclusions discussed below.

2.2. Computational Details. Spin-polarized density functional theory (DFT) calculations with a plane-wave basis set were performed using the Vienna Ab initio Simulation Package.[29−31] Two forms of the generalized gradient approximation functional were used to describe the exchange and correlation energy, Perdew−Wang 91 (PW91)[32] and revised Perdew−Burke−Ernzerhof (RPBE).[33] In the PW91 calculations, electron−ion interactions were treated with ultrasoft pseudopotentials,[34] while in the RPBE calculations, the projector augmented wave method[35] was employed. In all calculations, the energy cutoff of the plane wave basis set was 400 eV. The Brillouin zone was sampled using the Monkhorst−Pack scheme[36] with a 4 × 4 × 1 *k*-point mesh for the $p(2\times2)$ Pd(111) surface slab and a single *k*-point at (0 0.25 0) for the larger unit cell of Pd_5O_4 surface oxide. Optimized structures were obtained by minimizing the forces on each ion until they fell below 0.05 eV/Å. Transition states were determined with the climbing image nudged elastic band (CI-NEB) method.[37,38]

Structures of clean and adsorption Pd(111) surfaces were simulated within the supercell approach using slabs consisting of six layers. The positions of the bottom two layers were fixed during structure relaxation in the geometry of bulk Pd. Adsorbates were introduced on the top Pd(111) layer. Structures of the two-dimensional Pd_5O_4 surface oxide layer, as described in the Results section, are from a previous publication.[17] A 12 Å vacuum layer is used to separate periodic images of the slabs. The lattice constant of Pd used for building surface structures is computed to be 3.966 Å with PW91 and 3.982 Å with RPBE.

3. RESULTS

3.1. Chemisorption of O and CO on Pd(111). Previous experimental and theoretical work show that exposure of Pd(111) to oxygen gas results in two stable ordered surface structures: a $p(2\times2)$ overlayer with 0.25 monolayer (ML) coverage and a two-dimensional Pd_5O_4 surface oxide; both structures are considered in this work. On the $p(2\times2)$ Pd(111) surface, the preferred adsorption site for a single O atom (0.25 ML) is the fcc hollow site. The atomic structure of the Pd_5O_4 surface oxide, which has been proposed based on a combination of experimental and computational techniques, is shown in Figure 1. The unit cell of the surface oxide layer has dimensions of $(\sqrt{6}\times\sqrt{6})$ with respect to the unit cell of the Pd(111) substrate, as indicated by the blue square in Figure 1. The surface oxide has two types of Pd atoms, 2- and 4-fold coordinated to O atoms, as well as two types of O atoms, 3- and 4-fold coordinated to Pd atoms. The 4-fold oxygen is 0.8 Å lower in the *z* direction and is in direct contact with the Pd(111) substrate, whereas the 3-fold oxygen coordinates laterally with Pd atoms in the oxide layer. The binding energies of the above-mentioned surface structures are calculated with eq 5 as summarized in Table 2. The $p(2\times2)$-O^{fcc} overlayer is more stable than the Pd_5O_4 surface oxide but only by tens of meV/O. The oxygen coverage in Pd_5O_4 (0.8 ML) is higher than that of the $p(2\times2)$-O^{fcc} overlayer (0.25 ML) so that the surface oxide will in fact be more stable under oxygen-rich conditions. The binding energies of the $p(2\times2)$-O^{fcc} overlayer and Pd_5O_4 calculated in this work are higher (less stable) than the values reported (−1.36 eV/O for $p(2\times2)$-O^{fcc} overlayer and −1.24 eV/O for Pd_5O_4) in ref 17. The variation is likely due to the different computational settings employed. In recent

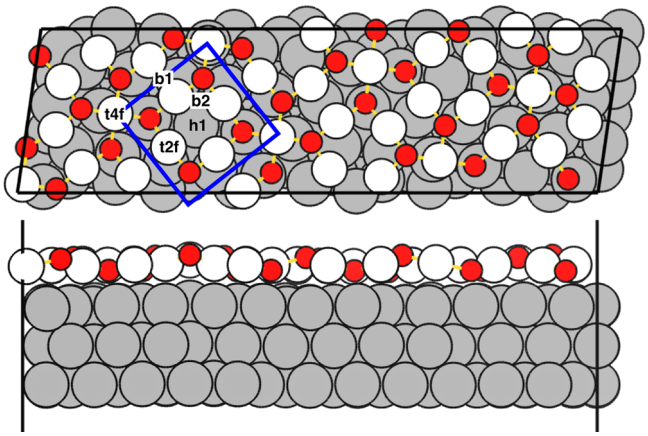

Figure 1. Top and side views of the Pd_5O_4 surface oxide. The supercell (black parallelogram) contains seven unit cells of Pd_5O_4 (blue square). Various adsorption sites in the unit cell are marked. Pd atoms in the surface oxide are white; Pd atoms in Pd(111) are dark gray; and the O atoms are red.

Table 2. Surface Structures with the Lowest Binding Energies on the $p(2\times2)$ Pd(111) Surface with Coverages Ranging from 0.25 to 1.0 ML[a]

		$\tilde{E}_{bind}$ (eV)	
	coverage (ML)	RPBE	PW91
pure O*:			
$p(2\times2)$-O^{fcc}	0.25	−1.05	−1.19
$p(2\times1)$-O^{fcc}	0.50	−0.77	−0.93
$(\sqrt{6}\times\sqrt{6})$ Pd_5O_4	0.80	−0.97	−1.13
pure CO*:			
$p(2\times2)$-CO^{hcp}	0.25	−1.58	−1.95
$(\sqrt{3}\times\sqrt{3})R30°$-$CO^{fcc}$	0.33	−1.62	−2.00
$c(4\times2)$-$2CO^{fcc,hcp}$	0.50	−1.45	−1.84
$p(2\times2)$-$3CO^{fcc,hcp,top}$	0.75	−1.08	−1.46
$p(1\times1)$-CO^{fcc}	1.00	−0.49	−0.96
mixed CO*/O*:			
(2×2)-O^{fcc}-CO^{fcc}	0.50	−2.03	−2.60
(2×2)-$2O^{fcc}$-CO^{fcc}	0.75	−1.85	−2.63
(2×2)-O^{fcc}-$2CO^{top,hcp}$	0.75	−2.60	−3.51
(2×2)-O^{fcc}-$3CO^{fcc}$	1.00	−1.89	−3.48
(2×2)-$2O^{fcc}$-$2CO^{fcc}$	1.00	−1.75	−3.06
(2×2)-$3O^{fcc}$-CO^{fcc}	1.00	−1.13	−2.17

[a]For surface structures with only CO or O, the binding energies are calculated per molecule; for mixed CO and O structures, total binding energies are given.

experimental work,[19] it was pointed out that the stability of the Pd_5O_4 surface oxide might be overestimated in ref 17. For comparison, the binding energy of the $p(2\times1)$-O^{fcc} overlayer is also included in Table 2. Experimentally, it is found that the phase boundary can be well-described by a line of constant chemical potential of $\mu_O = -1.24$ eV above 650 K.[19] The value of μ_O determined from our DFT calculations for the transition between the oxygen $p(2\times2)$ chemisorption phase and the Pd_5O_4 surface oxide phase is −1.1 eV with PW91 and −0.91 eV with RPBE, which are systematically above the experimental value. This discrepancy between the experimental and theoretical chemical potential gives rise to a 50 K (100 K for RPBE) error bar in temperature and a factor of 10^2 (10^4 for RPBE) error bar in pressure. Systematic errors of similar magnitude are found in a Ag/O system.[39] It can be seen that

dx.doi.org/10.1021/cs5006025 | ACS Catal. 2014, 4, 3435−3443

the binding strength decreases dramatically when the oxygen coverage increases from 0.25 to 0.5 ML, indicating a repulsive interaction between the adsorbed oxygen atoms. The Pd atoms in the Pd_5O_4 surface oxide screens the repulsive interaction between oxygen atoms, which results in the higher stability of the surface oxide at high oxygen coverage.

Experimental studies on CO adsorption on Pd(111) surface revealed that the $(\sqrt{3}\times\sqrt{3})R30°$, $c(4\times2)$-2CO, and (2×2)-3CO ordered phases are formed at coverages of 0.33 ML, 0.5 ML, and 0.75 ML.[40−44] On these surfaces, various adsorption sites (top, bridge, fcc, and hcp) and coverages of CO overlayer on Pd(111) are considered in this study using both the PW91 and RPBE functionals. RPBE is designed to generally improve binding energies of molecules to surfaces and specifically resolve the overbinding problem of CO on transition metal surfaces.[45] The most stable ordered CO adsorption phases at each coverage considered, along with the corresponding binding energies measured in eV/CO, are summarized in Table 2. Experimentally, the critical $\Delta\mu_{CO}$ corresponding to three different CO adsorption phase transitions in the CO/Pd(111) system can be extracted from the equilibrium pressure−temperature phase diagram in work from the Goodman group.[42] Comparing to experimental values ($\Delta\mu_{CO}$ ∼ −2.18, −1.58, −0.71 eV), DFT calculations with the PW91 functional ($\Delta\mu_{CO}$ ∼ −2.0, −1.52, −0.69 eV) show good agreement, whereas the RPBE functional predicts values that are systematically higher than experiment ($\Delta\mu_{CO}$ ∼ −1.62, −1.09, −0.33 eV). It is currently not understood how RPBE can improve the CO adsorption energy but fail to accurately predict the CO/Pd(111) phase diagram, while PW91 overbinds CO but reproduces the CO/Pd(111) phase diagram reasonably well. One possible stabilizing contribution to the adsorbed species is their entropy, which is neglected in the current approximation.

The adsorption of mixed O and CO ordered phases on the $p(2\times2)$ surface are shown in Table 2. It is found the repulsive interaction between O and CO is even stronger than that of O−O or CO−CO. At 0.5 ML coverage, the mixed O^{fcc}-CO^{fcc} phase is 0.7 eV less stable than the separate O^{fcc} and CO^{hcp} phases. Consequently, it can be expected that it is energetically favorable to have separated O and CO domains. This finding is in agreement with experiments showing the formation of separate O and CO domains when an O precovered surface is exposed to CO.[2]

The stability of the calculated surface structures, in constrained equilibrium with O_2 and CO in the gas phase, can be compared using the Gibbs free energy of adsorption as defined in eq 1. The most stable phases are shown in the surface diagram in Figure 2 as a function of O_2 and CO chemical potentials. In the lower-right corner of Figure 2, where both O_2 and CO chemical potentials are low, the clean Pd(111) surface is the most stable phase. If the O_2 chemical potential is kept low and the CO chemical potential is increased (along the x-axis), the most stable surface goes through three ordered phases, $(\sqrt{3}\times\sqrt{3})R30°$, $c(4\times2)$, and $p(2\times2)$, with increasing CO coverage of 0.33, 0.5, and 0.75 ML. If the O_2 chemical potential is increased (along the y-axis) while keeping the CO chemical potential low, first a $p(2\times2)$ overlayer appears on the Pd(111) surface, then a Pd_5O_4 surface oxide, and finally the PdO bulk oxide. No coadsorption structures with both CO and O_2 are observed on the phase diagram.

The technologically relevant gas phase conditions of O_2 and CO (p_{O_2}, p_{CO} = 1 atm, T = 300−600 K) for CO oxidation are

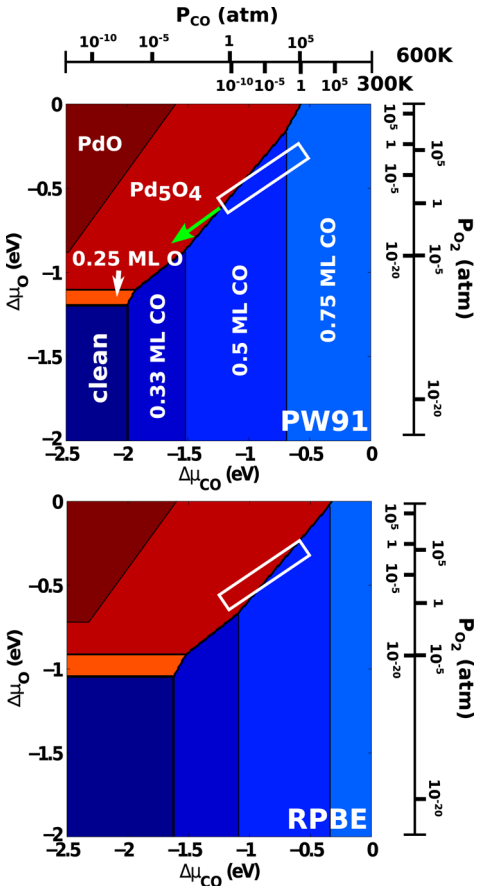

Figure 2. Surface phase diagram of the Pd(111) surface in constrained thermodynamic equilibrium with O_2 and CO in the gas phase. Surface states are annotated and differentiated by color. The white square marks the typical gas phase conditions of CO oxidation catalysis, i.e. partial pressures of 1 atm and temperatures of 300−600 K. The green arrow indicates an experimental path along which the surface changes from a metal to an oxide, as discussed later.

outlined with a white box in Figure 2. This region is near the boundary of the Pd_5O_4 surface oxide and the CO overlayer structures for both functionals considered. Considering the systematic errors in DFT for the O/Pd(111) and CO/Pd(111) adsorption energies mentioned above, the PW91 functional would give a surface phase diagram more consistent with experiments, whereas the RPBE functional systematically destabilizes the O/Pd(111) and CO/Pd(111) interactions. Taking these systematic errors into account, the white bar in Figure 2 remains close to the boundary of the Pd_5O_4 surface oxide and the CO overlayer structures. The constrained equilibrium approach used to construct the surface phase diagram neglects kinetic reactions between O_2 and CO and thus only indicates phases which might be relevant under reaction conditions. Kinetic considerations are required to understand the surface structures and reaction mechanism(s) under reaction conditions, especially at the O/CO phase boundaries where the reaction rate is expected to be high. On the right side of the boundary, the Pd(111) surface is covered and likely poisoned by CO, preventing O_2 activation on the metallic surface. Thus, knowledge of the activity of the Pd_5O_4 surface oxide is key for understanding reactivity at the phase boundary.

3.2. O and CO Adsorption on Pd_5O_4. The binding energies of O and CO to the Pd_5O_4 surface are calculated and

dx.doi.org/10.1021/cs5006025 | ACS Catal. 2014, 4, 3435−3443

compiled in Table 3. CO binds the most strongly on the b1 site—the bridge site between two 2-fold Pd atoms. The

Table 3. Calculated Binding Energies of CO and O on the Pd_5O_4 Surface Oxide

	E_{bind} (eV)	
	RPBE	PW91
CO adsorption:		
CO^{t4f}	0.04	−0.51
CO^{t2f}	−0.55	−0.62
CO^{b1}	−0.73	−1.08
CO^{b2}	−0.24	−0.73
CO^{h1}	−0.35	−0.43
O adsorption:		
O^{b1}	0.16	0.00
O^{h1}	0.02	−0.36

calculated CO binding energies at various sites are in good agreement with other published values.[46] The CO adsorption energy calculated PW91 is −1.08 eV, which is about 0.9 eV higher than that on the pristine Pd(111) surface with a 0.25 ML coverage. The CO binding energy calculated with RPBE (−0.73 eV) is even higher. Oxygen adsorbs to Pd_5O_4 to the b1 and h1 sites; the other sites are unstable. RPBE predicts positive binding energies on both sites, while PW91 predicts neutral and sightly negative binding energies on the b1 and h1 sites, respectively. Besides, the molecular O_2 adsorption energy on the b1 site is calculated to be −0.37 eV using PW91. Consequently, oxygen adsorption and activation on Pd_5O_4 is unlikely to occur. Weak O_2 adsorption on the Pd surface oxide is also observed in experiment.[47] Without oxygen adsorption, CO oxidation on Pd_5O_4 can only proceed with the participation of lattice oxygen in the Pd_5O_4 surface oxide layer, i.e. the MvK reaction mechanism.

3.3. CO Oxidation on the Pd_5O_4 Surface Oxide. The above discussion asserts that lattice oxygen in Pd_5O_4 can participate the CO oxidation reaction following the MvK reaction mechanism. This can proceed in two ways, namely the Langmuir−Hinshelwood (LH) or Eley−Rideal (ER) mechanisms. In the LH mechanism, a CO molecule adsorbs on the Pd_5O_4 surface oxide before it reacts with a lattice oxygen, while in the ER mechanism, CO reacts with a lattice oxygen directly from the gas-phase. In order to determine which reaction mechanism is more favorable, the reaction rates of the two candidate mechanisms need to be calculated.

As a first step in computing the reaction rate of CO oxidation on Pd_5O_4, energy barriers of the relevant catalytic processes are calculated with the CI-NEB method. For the LH mechanism, the adsorbed CO molecule is considered to reside on the preferential b1 site. The adsorbed CO molecule can then react with the 4- or 3-fold O, as shown in Figures 3(a) and (b), respectively. The reaction barriers of both processes are above 0.9 eV so that the Pd_5O_4 surface oxide is not expected to be active for CO oxidation at low temperature. At higher temperatures where such barriers can be overcome, the reaction rate will be limited by a CO coverage on the Pd_5O_4 surface due to weak binding. These expectations are quantified using a microkinetic analysis later in this study. The MEP of the ER reaction between a gas-phase CO molecule and the 3-fold lattice oxygen is shown in Figure 3(c). In our CI-NEB calculation, the gas-phase CO molecule is first attracted to a 2-fold Pd atom and chemically adsorbs atop the Pd atom before reacting with a neighboring 3-fold oxygen, overcoming an energy barrier of 0.62 eV. In this regard, the mechanism is not strictly ER, but since the binding energy of the absorbed state is

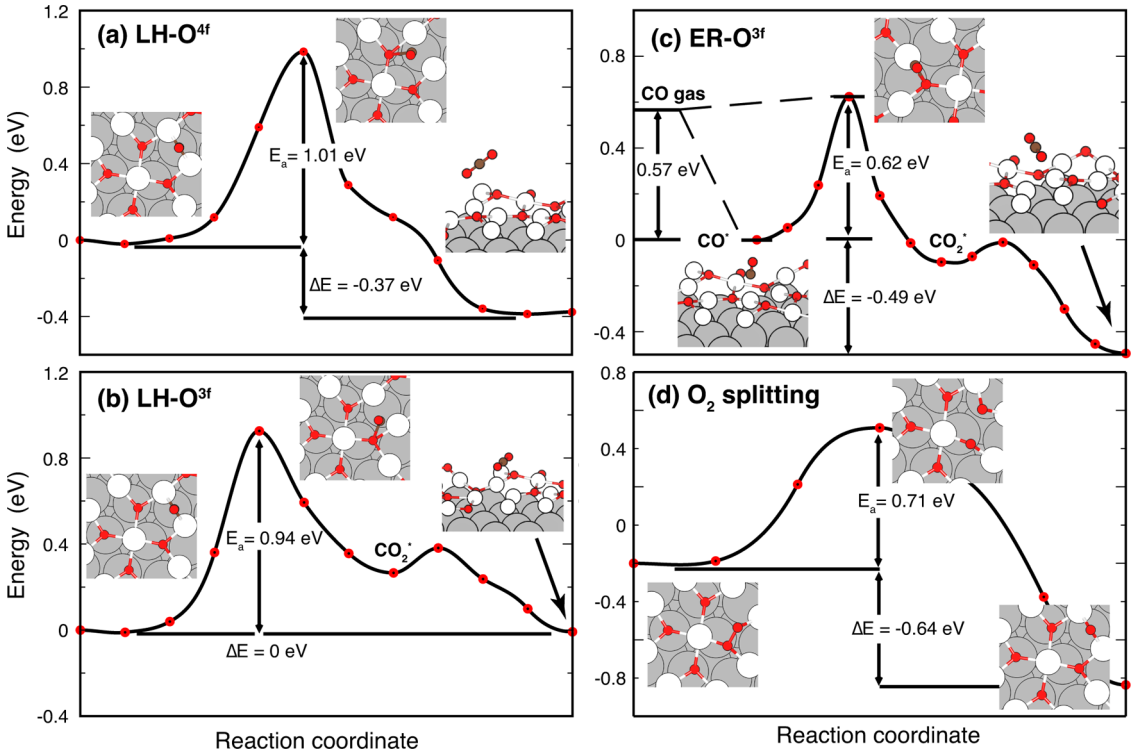

Figure 3. Minimum energy paths (MEPs) of reactions over Pd_5O_4: (a) adsorbed CO reacts with 4-fold oxygen; (b) adsorbed CO reacts with 3-fold oxygen; (c) gas-phase CO reacts with 3-fold oxygen; and (d) O_2 dissociation at a surface oxygen vacancy.

dx.doi.org/10.1021/cs5006025 | ACS Catal. 2014, 4, 3435−3443

overwhelmed by the gas-phase entropy at the temperature of interest near 500 K, the CO molecule is over 10^6 times more likely to approach react from the gas phase (ER) than from the adsorbed state (LH). Using the gas-phase reference energy for CO gives a ER barrier of only 0.05 eV.

Lattice oxygen atoms on Pd_5O_4 consumed during the CO oxidation reaction can be replenished by the dissociative adsorption of gas phase O_2 molecules at oxygen vacancies. Figure 3(d) shows the MEP of the O−O bond splitting process of an O_2 molecule adsorbed on a vacancy site originally filled with a 3-fold oxygen atom. The energy barrier of the oxygen replenishing process is computed to be 0.72 eV. After O−O splitting, one O atom fills the vacancy, and the second adsorbs to the b1 site. This adsorbed oxygen atom at the b1 site is weakly bound and will rapidly combine with CO.

Although the energy barrier of the ER mechanism is lower than that of the LH mechanism, enthalpy is not the only factor in determining their relative reaction rate. The reactant's surface coverage in the LH mechanism and small pre-exponential factor[5] in the ER mechanism should also be considered. Accordingly, a microkinetic model is employed to take these factors into account and calculate the overall reaction rates via the two mechanisms. The reaction rates of CO oxidation on Pd_5O_4 through the LH and the ER mechanism are computed as

$$r_{LH}^{Pd_5O_4} = k_{LH}^{Pd_5O_4}\theta_{CO}^{Pd_5O_4} \quad (7)$$

and

$$r_{ER}^{Pd_5O_4} = k_{ER}^{Pd_5O_4}p_{CO} \quad (8)$$

where k is the rate constant, θ_{CO} is the coverage of CO molecule on Pd_5O_4, and p_{CO} is the partial pressure of CO. In eqs 7 and 8, the concentration of the product, CO_2, is assumed to be low so that the reverse reaction is neglected. Another simplification is that the replenishment of the lattice oxygen is assumed to be fast so that the concentration of oxygen vacancies is zero. The rate constant k is calculated as

$$k = \frac{k_B T}{h}\exp\left(\frac{\Delta S^{\ddagger}}{k_B}\right)\exp\left(\frac{-E_a}{k_B T}\right) \quad (9)$$

In the LH mechanism, $\Delta S^{\ddagger}$ is essentially zero, whereas in the ER mechanism $\Delta S^{\ddagger}$ is approximated by the entropy of the gas-phase CO molecule. The energy barrier (E_a) is 0.94 and 0.05 eV for LH and ER mechanisms, respectively. Adsorption and desorption of CO on Pd_5O_4 is considered to be in equilibrium, so that the CO coverage on Pd_5O_4 is given by the Langmuir adsorption model where $\theta_{CO}^{Pd_5O_4}$ is calculated as

$$\theta_{CO} = \frac{K_{CO}^{Pd_5O_4}p_{CO}}{1 + K_{CO}^{Pd_5O_4}p_{CO}} \quad (10)$$

In this expression, $K = e^{-(E_b - T\Delta S)/k_B T}$ is the adsorption equilibrium constant of CO on Pd_5O_4, and E_b is the binding energy, which is taken to be the RPBE calculated value of −0.73 eV. ΔS is the entropy change of adsorption, which is approximated as the entropy of the gas-phase molecule. For T = 500 K and p_{CO} = 1 atm, the reaction rate of the ER mechanism is calculated to be 43 times larger than that of the LH mechanism. This result, however, is sensitive to the CO adsorption energy; using the −1.08 eV value calculated by the PW91 functional, the preferred reaction mechanism changes to the LH mechanism (50 times faster than the ER mechanism) due to the significant increase in CO coverage. Since the CO adsorption energy is known to be overestimated by PW91, and RPBE is formulated to improve the overbinding problem, we believe the RPBE value to be more accurate.

The microkinetic modeling predicts that the ER reaction mechanism is preferred on Pd_5O_4. However, due to the uncertainty of our DFT-calculated CO adsorption energies and possible missing entropic contributions to our assumed pre-exponential prefactors,[48] the case for the ER mechanism over LH is not conclusive from the calculations alone. Additional evidence from experiment, however, does make a compelling case. Experimentally, the reactive oxygen species is determined to be the 3-fold oxygen in the Pd_5O_4 surface oxide layer, and CO is not observed to be present on the surface oxide when the high reactivity is observed.[10,16] Additionally, CO oxidation occurs over the Pd_5O_4 at temperatures as low as 330 K.[22] At such low temperatures, the high-barrier LH mechanism is unfavored. These experimental observations are in support of our calculated ER mechanism. Combining these theoretical and experimental results, we can conclude that the ER mechanism is preferred.

3.4. Stability of the Pd_5O_4 Surface Oxide. Although the Pd_5O_4 surface oxide is reactive via the ER reaction mechanism, it is possible that it will decompose to metastable oxygen-rich phases when the oxygen vacancy concentration reaches a threshold value. Kinetically, the decomposition of Pd_5O_4 is governed by the relative rates of oxygen vacancy formation by CO oxidation and vacancy filling by O_2 dissociative adsorption. From the microkinetic model, the steady state oxygen vacancy concentration can be estimated as $r_{ER}^{Pd_5O_4}/k_{O_2}^{diss}$, when the rate of formation and filling are set equal. The oxygen vacancy concentration is plotted as a function of temperature and CO partial pressure in Figure 4, where the rate constant of O_2 dissociation ($k_{O_2}^{diss}$) is calculated from the 0.71 eV reaction barrier shown in Figure 3(d). Under conditions of interest, oxygen vacancy filling is much faster that CO oxidation, and the steady-state concentration is as low as 10^{-5} so that the decomposition of Pd_5O_4 surface oxide is unlikely. It is still possible, however, for CO covered Pd(111) and Pd_5O_4 surface oxide to coexist at the conditions indicated by their common phase boundary line in the surface phase diagram. Hence, Pd_5O_4 could be reduced at the coexisting phase boundary as illustrated by Hammer and co-workers[49,50] and confirmed in experiments on Pd(100).[51]

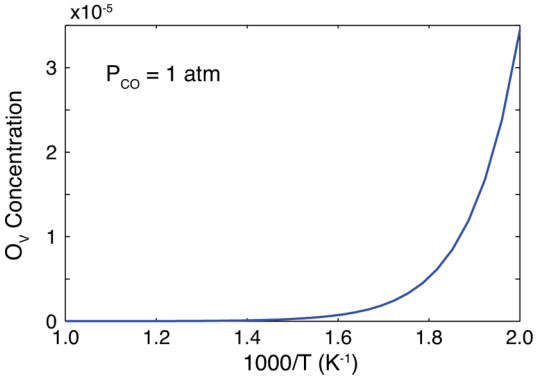

Figure 4. Oxygen vacancy concentration on the Pd_5O_4 surface oxide as a function of temperature, for a CO partial pressure of 1 atm.

dx.doi.org/10.1021/cs5006025 | ACS Catal. 2014, 4, 3435−3443

3.5. CO Oxidation over Pd(111). To complete the picture of CO oxidation on the Pd(111) surface, the microkinetic analysis employed in ref 52 is included. The following microkinetic equations are used to calculate the reaction rate of CO oxidation on metallic Pd(111)

$$r_{LH}^{Pd(111)} = k_{LH}^{Pd(111)} \theta_{CO}^{Pd(111)} \theta_{O}^{Pd(111)} \quad (11)$$

$$r_{O_2}^{diss} = k_{O_2}^{diss} \theta_{O_2} \theta_* \quad (12)$$

$$\theta_{CO} = \frac{K_{CO}^{Pd(111)} p_{CO}}{1 + K_{CO}^{Pd(111)} p_{CO} + K_{O_2}^{Pd(111)} p_{O_2}} \quad (13)$$

$$\theta_{O_2} = \frac{K_{O_2}^{Pd(111)} p_{O_2}}{1 + K_{CO}^{Pd(111)} p_{CO} + K_{O_2}^{Pd(111)} p_{O_2}} \quad (14)$$

$$\theta_* = \frac{1}{1 + K_{CO}^{Pd(111)} p_{CO} + K_{O_2}^{Pd(111)} p_{O_2}} \quad (15)$$

We now assume that the formation of O* is in steady state and thus that $r_{LH}^{Pd(111)} = 1/2(r_{O_2}^{diss})$. The adsorption energies of CO and O_2 are based upon calculations of a 1/4 ML coverage with the RPBE functional. Arrhenius plots of CO_2 formation at experimental gas-pressures[23] both on metallic Pd(111) and the Pd_5O_4 surface are in Figure 5. On the metallic Pd(111) surface

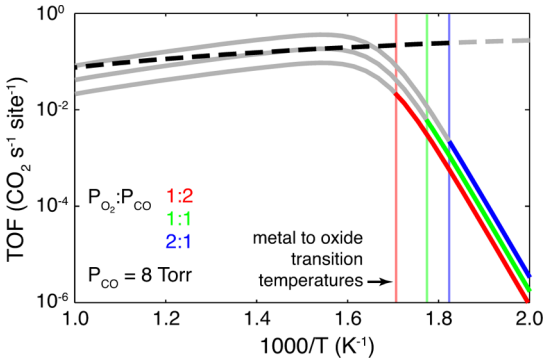

Figure 5. Arrhenius plots of CO_2 formation at various gas pressures both on metallic Pd(111) surface (solid line) and on Pd_5O_4 surface oxide (dashed line). The vertical lines indicate the transition temperature between a stable metal surface at low temperature and the Pd_5O_4 oxide phase at high temperature, in a p_{CO} = 8 Torr environment. The dark-colored portions of the curves indicate the reaction rates on the stable surface.

at low temperature, the CO oxidation activity is limited by CO desorption. The CO poisoning effect is also seen in the decreasing reactivity with increasing CO partial pressure at low temperature. The rate of CO_2 formation reaches a maximum value when the CO coverage on Pd(111) reaches about 0.2 ML. At higher temperatures, reactivity decreases because CO and O_2 molecules cannot effectively adsorb on the metal surface. At this stage, the Pd(111) surface is essentially clean according to our microkinetic modeling if no phase transition is taken into account. As a result, reactivity is limited by the low CO and O coverage. On the Pd_5O_4 surface oxide, CO oxidation activity decreases monotonically with increasing temperature because entropy favors gas phase CO and lowers the rate of the ER mechanism. CO inhibition does not play a role on Pd_5O_4, so that the activity is simply proportional to the CO partial pressure, as can be seen in eq 8. Figure 5 shows that the Pd(111) surface can have higher activity than the Pd_5O_4 surface oxide at high temperature; however, the assignment of the more reactive phase is coupled with which phase is stable under catalytic conditions.

Inspecting the experimental Arrhenius plots of CO_2 formation on Pt-group metals including Pd(100), Pt(110), Rh(111), there exists three phases for the kinetics of CO oxidation: (1) a CO inhibited phase, (2) a "hyperactive" phase, and (3) a high temperature, mass transfer limited phase.[7,23−25] The kinetic behavior of the CO inhibited phase and the high-temperature, mass-transfer limited phases resemble the metallic Pd(111) and the Pd_5O_4 surface oxide in our microkinetic analysis, as shown in Figure 5. The similarity with our theoretical results suggests a materials transition from a metallic surface to a surface oxide with increasing temperature. A materials transition is also supported by the DFT-calculated surface phase diagram. Using experimental gas pressure of p_{CO} = 8 Torr, p_{O_2} = 4 Torr and changing temperature from 500 to 800 K[23] will result in a path on the surface phase diagram starting from the metallic phase to the surface oxide as indicated by the green arrow in Figure 2. Although, as seen in Figure 5, the LH reaction mechanism on metallic Pd(111) surface also has negative apparent activation energy at high temperature, the decreasing rate of activity with increasing temperature is more pronounced than on Pd_5O_4 following the ER reaction mechanism. This is also observed in experiment; the decreasing slope in activity flattens when going from UHV to high pressure conditions, where the surface oxide is expected to be present.[23] The relationship between material transition and change of kinetic behavior on Pd(100) surface is also evidenced from the experimental study by using surface X-ray diffraction (SXRD) coupled with a flow reactor.[7] In the experiment, using SXRD to distinguish between metallic and oxidized Pd(100) surface, dramatically different kinetic behaviors are found between the metal and oxide surfaces. Although, experimentally, the slowly decreasing CO_2 formation rate with respect to increasing temperature is attributed to be mass transfer limitations, our theoretical results using DFT-parametrized microkinetic model suggest that this kinetic behavior is a result of the CO oxidation following the ER reaction mechanism on the surface oxide. Experimentally, at a high p_{O_2}:p_{CO} ratio, the kinetic behavior at high temperature deviates from those at a low p_{O_2}:p_{CO} ratio.[23−25] The most obvious example is CO oxidation over Pd(100) surface. The difference is likely due to the formation of thick oxide film on the metal surface. From a theoretical point of view, it has been found that a thick PdO film has distinct properties from a monolayer PdO surface oxide.[53] Importantly, the CO binding energy on the PdO(101) surface is much stronger than that on the $(\sqrt{5}\times\sqrt{5})R27°$ surface oxide over Pd(100),[5,13] which should change the reaction mechanism.

Finally, we turn our attention to the nature of the "hyperactive" phase. This phase is seen experimentally between the CO-inhibited phase and the so-called mass transfer limited phase. As can be seen in the surface phase diagram in Figure 2, the presence of the "hyperactive" phase coincides with the phase coexisting boundary between the CO covered Pd(111) surface and the Pd_5O_4 surface oxide. In both regions, the rate of CO oxidation reaction is expected to be low either due to overly weak or strong adsorption. In the phase coexistence

dx.doi.org/10.1021/cs5006025 | ACS Catal. 2014, 4, 3435−3443

region, it is conceivable that the interplay between surface oxide formation, decomposition, and CO adsorption makes available surface phases that are reactive toward CO oxidation. For instance, the oxygen atom in the surface oxide could be reduced by adsorbed CO at the reduced surface as shown both experimentally[51] and theoretically.[49,50] Consequently, surface oxide at the perimeter region is destabilized at the coexisting interface and then reduced to metastable oxygen-containing phases, such as the 0.25 or 0.5 ML phases. Upon exposure to CO, these metastable oxygen-containing domains, resulting from surface oxide decomposition, would reorganize with CO-containing domains forming various coadsorption phases that cannot be accessible directly through CO and O_2 chemisorption.[3] The reaction kinetics of these coadsorption phases are expected to be much faster than the CO-inhibited metal surface, which is evidenced from experimental studies of the reaction mechanism on O-covered Pd(111) surfaces.[1,2]

4. CONCLUSIONS

The most stable surface structures formed on Pd(111) have been investigated in constrained thermodynamics equilibrium with O_2 and CO in gas phase. A surface phase diagram is constructed from the stability of various chemisorption phases, surface oxides, and the bulk oxide under various gas-phase conditions. According to the phase diagram, a catalytically active region is identified at the phase boundary between the Pd_5O_4 surface oxide and the CO-covered metallic surface.

The constrained equilibrium approach neglects the kinetic formation of CO_2, so the reaction kinetics of CO oxidation over Pd_5O_4 is examined by calculating the reaction barriers of relevant processes. It is found that oxygen atom weakly adsorbs on Pd_5O_4 so that CO can only react with lattice oxygen via the MvK mechanism. The CO oxidation though the LH reaction mechanism is calculated to have an energy barrier about 0.9 eV. CO can also react with a 3-fold lattice oxygen in Pd_5O_4 with the ER mechanism with only 0.05 eV. The 3-fold oxygen vacancy generated on the surface oxide is replenished with O_2 splitting with a barrier of 0.71 eV. Using a microkinetic analysis with DFT-calculated adsorption energies and energy barriers, the favorable CO oxidation mechanism on Pd_5O_4 surface oxide is determined to be the ER mechanism.

The microkinetic analysis is also used to illustrate the distinct trends in activity for the metallic Pd(111) surface and the Pd_5O_4 surface oxide. At low temperature, the Pd(111) surface is more stable, and CO oxidation occurs slowly due to CO-poisoning via the LH mechanism. Above 500−600 K (depending upon CO and O_2 pressure), a material transition occurs to the Pd_5O_4 surface oxide and CO oxidation occurs uninhibited by CO via the ER mechanism. The kinetics of CO oxidation predicted from microkinetic analysis agrees well with experimental measurements. Previously, experimentalists have explained the kinetics of the CO-uninhibited region by using mass transfer limited argument. However, through our theoretical study, we show that the slowing decreasing CO_2 formation rate with increasing temperature is a consequence of the ER mechanism on the surface oxide.

The experimentally observed "hyperactive" phase is explained by the coexisting of a CO covered metal surface with the surface oxide. In this region, due to the interplay between surface oxide formation, decomposition, and CO adsorption, many CO oxidation active surface structures can lead to high catalytic activity. Under technologically relevant conditions, the Pd_5O_4 surface oxide and the CO-covered metallic surface coexist with each other as predicted by the surface phase diagram, which explains the high reactivity of Pd catalysts.

AUTHOR INFORMATION

Corresponding Author

*E-mail: henkelman@cm.utexas.edu.

Notes

The authors declare no competing financial interest.

ACKNOWLEDGMENTS

This work is supported by the Department of Energy under contract DE-FG02-13ER16428 and the Welch Foundation under grant F-1841. The calculations were done at the National Energy Research Scientific Computing Center and the Texas Advanced Computing Center.

REFERENCES

(1) Nakai, I.; Kondoh, H.; Shimada, T.; Resta, A.; Andersen, J. N.; Ohta, T. *J. Chem. Phys.* **2006**, *124*, 224712.
(2) Kim, S. H.; Méndez, J.; Wintterlin, J.; Ertl, G. *Phys. Rev. B* **2005**, *72*, 155414.
(3) Méndez, J.; Kim, S. H.; Cerdá, J.; Wintterlin, J.; Ertl, G. *Phys. Rev. B* **2005**, *71*, 085409.
(4) Zhang, C. J.; Hu, P. *J. Am. Chem. Soc.* **2001**, *123*, 1166−1172.
(5) Hirvi, J. T.; Kinnunen, T.-J. J.; Suvanto, M.; Pakkanen, T. A.; Nørskov, J. K. *J. Chem. Phys.* **2010**, *133*, 084704.
(6) Hendriksen, B.; Bobaru, S.; Frenken, J. *Surf. Sci.* **2004**, *552*, 229−242.
(7) van Rijn, R.; Balmes, O.; Resta, A.; Wermeille, D.; Westerstrom, R.; Gustafson, J.; Felici, R.; Lundgren, E.; Frenken, J. W. M. *Phys. Chem. Chem. Phys.* **2011**, *13*, 13167−13171.
(8) Hendriksen, B. L. M.; Ackermann, M. D.; van Rijn, R.; Stoltz, D.; Popa, I.; Balmes, O.; Resta, A.; Wermeille, D.; Felici, R.; Ferrer, S.; Frenken, J. W. M. *Nat. Chem.* **2010**, *2*, 730−734.
(9) Toyoshima, R.; Yoshida, M.; Monya, Y.; Suzuki, K.; Mun, B. S.; Amemiya, K.; Mase, K.; Kondoh, H. *J. Phys. Chem. Lett.* **2012**, *3*, 3182−3187.
(10) Blomberg, S.; Hoffmann, M. J.; Gustafson, J.; Martin, N. M.; Fernandes, V. R.; Borg, A.; Liu, Z.; Chang, R.; Matera, S.; Reuter, K.; Lundgren, E. *Phys. Rev. Lett.* **2013**, *110*, 117601.
(11) Todorova, M.; Lundgren, E.; Blum, V.; Mikkelsen, A.; Gray, S.; Gustafson, J.; Borg, M.; Rogal, J.; Reuter, K.; Andersen, J.; Scheffler, M. *Surf. Sci.* **2003**, *541*, 101−112.
(12) Kostelník, P.; Seriani, N.; Kresse, G.; Mikkelsen, A.; Lundgren, E.; Blum, V.; Šikola, T.; Varga, P.; Schmid, M. *Surf. Sci.* **2007**, *601*, 1574−1581.
(13) Rogal, J.; Reuter, K.; Scheffler, M. *Phys. Rev. B* **2007**, *75*, 205433.
(14) Rogal, J.; Reuter, K.; Scheffler, M. *Phys. Rev. Lett.* **2007**, *98*, 046101.
(15) Rogal, J.; Reuter, K.; Scheffler, M. *Phys. Rev. B* **2008**, *77*, 155410.
(16) Toyoshima, R.; Yoshida, M.; Monya, Y.; Kousa, Y.; Suzuki, K.; Abe, H.; Mun, B. S.; Mase, K.; Amemiya, K.; Kondoh, H. *J. Phys. Chem. C* **2012**, *116*, 18691−18697.
(17) Lundgren, E.; Kresse, G.; Klein, C.; Borg, M.; Andersen, J. N.; De Santis, M.; Gauthier, Y.; Konvicka, C.; Schmid, M.; Varga, P. *Phys. Rev. Lett.* **2002**, *88*, 246103.
(18) Ketteler, G.; Ogletree, D. F.; Bluhm, H.; Liu, H.; Hebenstreit, E. L. D.; Salmeron, M. *J. Am. Chem. Soc.* **2005**, *127*, 18269−18273.
(19) Kasper, N.; Nolte, P.; Stierle, A. *J. Phys. Chem. C* **2012**, *116*, 21459−21464.
(20) Zheng, G.; Altman, E. I. *J. Phys. Chem. B* **2002**, *106*, 1048−1057.
(21) Chen, M.; Cai, Y.; Yan, Z.; Gath, K.; Axnanda, S.; Goodman, D. W. *Surf. Sci.* **2007**, *601*, 5326−5331.
(22) Gabasch, H.; Knop-Gericke, A.; Schlogl, R.; Borasio, M.; Weilach, C.; Rupprechter, G.; Penner, S.; Jenewein, B.; Hayek, K.; Klotzer, B. *Phys. Chem. Chem. Phys.* **2007**, *9*, 533−540.

(23) Gao, F.; McClure, S.; Cai, Y.; Gath, K.; Wang, Y.; Chen, M.; Guo, Q.; Goodman, D. *Surf. Sci.* **2009**, *603*, 65−70.
(24) Gao, F.; Wang, Y.; Cai, Y.; Goodman, D. W. *J. Phys. Chem. C* **2009**, *113*, 174−181.
(25) Chen, M.; Wang, X. V.; Zhang, L.; Tang, Z.; Wan, H. *Langmuir* **2010**, *26*, 18113−18118.
(26) Reuter, K.; Scheffler, M. *Phys. Rev. B* **2003**, *68*, 045407.
(27) Chase, M. W.; Davis, C. A.; Downey, J. R.; Frurip, D. J.; McDonald, R. A.; Syverud, A. N. *J. Phys. Chem. Ref. Data* **1985**, *14*.
(28) Campbell, C. T.; Sellers, J. R. V. *J. Am. Chem. Soc.* **2012**, *134*, 18109−18115.
(29) Kresse, G.; Hafner, J. *Phys. Rev. B* **1993**, *47*, 558.
(30) Kresse, G.; Furthmüller, J. *Comput. Mater. Sci.* **1996**, *6*, 15−50.
(31) Kresse, G.; Furthmüller, J. *Phys. Rev. B* **1996**, *54*, 11169.
(32) Perdew, J. P.; Wang, Y. *Phys. Rev. B* **1992**, *45*, 13244.
(33) Hammer, B.; Hansen, L. B.; Nørskov, J. K. *Phys. Rev. B* **1999**, *59*, 7413−7421.
(34) Kresse, G.; Joubert, D. *Phys. Rev. B* **1999**, *59*, 1758−1775.
(35) Blöchl, P. E. *Phys. Rev. B* **1994**, *50*, 17953.
(36) Monkhorst, H. J.; Pack, J. D. *Phys. Rev. B* **1976**, *13*, 5188−5192.
(37) Henkelman, G.; Jónsson, H. *J. Chem. Phys.* **2000**, *113*, 9978−9985.
(38) Henkelman, G.; Uberuaga, B. P.; Jónsson, H. *J. Chem. Phys.* **2000**, *113*, 9901−9904.
(39) Li, W.-X.; Stampfl, C.; Scheffler, M. *Phys. Rev. B* **2003**, *68*, 165412.
(40) Hoffmann, F. M. *Surf. Sci. Rep.* **1983**, *3*, 107−192.
(41) Bradshaw, A.; Hoffmann, F. *Surf. Sci.* **1978**, *72*, 513−535.
(42) Kuhn, W.; Szanyi, J.; Goodman, D. *Surf. Sci.* **1992**, *274*, L611−L618.
(43) Giebel, T.; Schaff, O.; Hirschmugl, C.; Fernandez, V.; Schindler, K.-M.; Theobald, A.; Bao, S.; Lindsay, R.; Berndt, W.; Bradshaw, A.; Baddeley, C.; Lee, A.; Lambert, R.; Woodruff, D. *Surf. Sci.* **1998**, *406*, 90−102.
(44) Rose, M.; Mitsui, T.; Dunphy, J.; Borg, A.; Ogletree, D.; Salmeron, M.; Sautet, P. *Surf. Sci.* **2002**, *512*, 48−60.
(45) Feibelman, P. J.; Hammer, B.; Nøskov, J. K.; Wagner, F.; Scheffler, M.; Stumpf, R.; Watwe, R.; Dumesic, J. *J. Phys. Chem. B* **2001**, *105*, 4018−4025.
(46) Martin, N. M.; Van den Bossche, M.; Grnbeck, H.; Hakanoglu, C.; Zhang, F.; Li, T.; Gustafson, J.; Weaver, J. F.; Lundgren, E. *J. Phys. Chem. C* **2014**, *118*, 1118−1128.
(47) Hinojosa, J. A., Jr.; Kan, H. H.; Weaver, J. F. *J. Phys. Chem. C* **2008**, *112*, 8324−8331.
(48) Campbell, C. T.; Árnadóttir, L.; Sellers, J. R. V. *Z. Phys. Chem.* **2013**, *227*, 1435−1454.
(49) Li, W.; Hammer, B. *Chem. Phys. Lett.* **2005**, *409*, 1−7.
(50) Westerström, R.; Wang, J. G.; Ackermann, M. D.; Gustafson, J.; Resta, A.; Mikkelsen, A.; Andersen, J. N.; Lundgren, E.; Balmes, O.; Torrelles, X.; Frenken, J. W. M.; Hammer, B. *J. Phys.: Condens. Matter* **2008**, *20*, 184018.
(51) Fernandes, V.; Gustafson, J.; Svenum, I.-H.; Farstad, M.; Walle, L.; Blomberg, S.; Lundgren, E.; Borg, A. *Surf. Sci.* **2014**, *621*, 31−39.
(52) Falsig, H.; Hvolbæk, B.; Kristensen, I. S.; Jiang, T.; Bligaard, T.; Christensen, C. H.; Nørskov, J. K. *Angew. Chem., Int. Ed.* **2008**, *47*, 4835−4839.
(53) Seriani, N.; Harl, J.; Mittendorfer, F.; Kresse, G. *J. Chem. Phys.* **2009**, *131*, 054701.